 CMES, vol.10, no.3, pp.217-228, 2005

An Implicit Integration Scheme for a Nonisothermal Viscoplastic, Nonlinear Kinematic Hardening Model

M. Akamatsu [1], K. Nakane [2], and N. Ohno [1,2]

Abstract: In this study, a fully implicit integration scheme is developed for a nonisothermal viscoplastic, nonlinear kinematic hardening model. Nonlinear dynamic recovery in addition to strain hardening is assumed for the evolution of multiple back stresses so that ratcheting and mean-stress relaxation can be properly simulated. Temperature dependence of back stress evolution is also taken into account in the constitutive model. By discretizing a set of such advanced constitutive relations using the backward Euler method, a tensor equation is derived and linearized to iteratively achieve the implicit integration of constitutive variables. The fully implicit integration scheme developed is programmed as a subroutine in a finite element code by assuming a power-law of dynamic recovery. Nonisothermal numerical examples are then given to demonstrate the performance of the implicit integration scheme.

keyword: Implicit integration, Viscoplasticity, Nonlinear kinematic hardening, Nonisothermal loading.

1 Introduction

Engineering has been demanding the implementation of advanced constitutive models in finite element methods. This needs to be done in accordance with the framework adopted for solving a global system of nonlinear, nodal force equilibrium equations. The Newton-Raphson method is usually employed to solve the nonlinear, nodal force equilibrium equations, since this method allows quadratic convergence. Then, the so-called consistent tangent modulus, i.e., the tangent derivative of discretized constitutive relations, is necessary to realize the quadratic convergence afforded by the Newton-Raphson method [Simo and Taylor (1985, 1986); Simo and Hughes (1998)]. Moreover, appropriate schemes for implicitly integrating stress, such as return mapping algorithms, are desired to attain the computational stability for large increments in finite element analysis [Simo and Taylor (1985, 1986); Simo and Hughes (1998)]. The implicit formulation based on consistent tangent operators is also effective for boundary element methods [Miers and Telles (2004)].

One of the well-known models of cyclic plasticity is the nonlinear kinematic hardening model proposed by Armstrong and Frederick (1966), which was also derived by Watanabe and Atluri (1986) using the endochronic theory. This model is highly rated, because it is based on a physical mechanism of strain hardening and dynamic recovery, and because it has the capability of representing well the shapes of stress-strain hysteresis loops. The Armstrong and Frederick model, however, has a serious drawback with respect to simulating ratcheting and mean-stress relaxation, which are fundamental phenomena in cyclic plasticity: their model may overpredict ratcheting up to a factor of ten [Ohno (1990)]. This problem can be overcome by reducing the effect of dynamic recovery relative to that of strain hardening, as was demonstrated by Chaboche (1991), Ohno and Wang (1993, 1994), Jiang and Sehitoglu (1996), and so forth. Hence, it is necessary to consider a more sophisticated form of nonlinear kinematic hardening than the Armstrong and Frederick model.

There have been two distinctive approaches for the implicit integration of nonlinear kinematic hardening models based on strain hardening and dynamic recovery. One is to reduce discretized constitutive relations to a nonlinear scalar equation. Such a nonlinear scalar equation was derived for the Armstrong and Frederick model by Hartmann and Haupt (1993) and was recently employed to implement more sophisticated nonlinear kinematic hardening models by Kobayashi and Ohno (2002). This approach was applied to rate-dependent models [Hartmann, Lührs and Haupt (1997); Kobayashi et al. (2003)]. It is however noted that the nonlinear scalar

[1] Department of Mechanical Science and Engineering, Nagoya University, Chikusa-ku, Nagoya 464-8603, Japan

[2] Department of Computational Science and Engineering, Nagoya University, Chikusa-ku, Nagoya 464-8603, Japan

equation becomes seriously complicated if dynamic recovery is nonlinear, resulting in inapplicability of the Newton-Raphson method to solving it [Kobayashi and Ohno (2002); Kobayashi et al. (2003)]. The other approach is to linearize discretized constitutive relations so that the plastic corrector in return mapping can be iteratively determined. This linearization approach was introduced for the Armstrong and Frederick model by Doghri (1993) and Sawyer, Wang and Jones (2001) and then extended to a specific case of weighted dynamic recovery by Hu and Wang (2003), yet restricted to isothermal rate-independent models. It is therefore of interest to employ the linearization approach for implementing nonisothermal rate-dependent, nonlinear kinematic hardening models.

In this study, using the linearization approach mentioned above, a fully implicit integration scheme is developed for a nonisothermal viscoplastic, nonlinear kinematic hardening model with multiple back stresses. Nonlinear dynamic recovery is assumed for the evolution of each back stress to simulate well ratcheting and mean-stress relaxation. Temperature dependence of back stress evolution is also taken into account, as was discussed by Chaboche (1986), Ohno and Wang (1991), and McDowell (1992). A set of such sophisticated constitutive relations are discretized using the backward Euler method. A resulting tensor equation is linearized by introducing the derivatives of discretized inelastic strain and multiple back stresses so that the implicit integration of constitutive variables can be iteratively achieved. The implicit integration scheme developed is programmed as a subroutine in a finite element code by assuming the nonlinearity of dynamic recovery suggested by Ohno and Wang (1993, 1994). Nonisothermal numerical examples are then given to verify the implicit integration scheme.

Throughout the paper, $(\dot{})$ indicates the differentiation with respect to time t, $(:)$ the inner product between tensors, $\otimes$ the tensor product, and $\|\|$ the Euclidean norm of second rank tensors, i.e., $\|\mathbf{x}\| = (\mathbf{x}:\mathbf{x})^{1/2}$.

2 Constitutive relations

We deal with elastic-viscoplastic materials which are initially isotropic and subjected to nonisothermal loading. Let us assume that strain ε is small and consists of thermal and mechanical parts, and that the mechanical part ε^m is additively further decomposed into elastic and viscoplastic parts, ε^e and ε^p. Moreover, it is assumed that ε^e obeys Hooke's law, while the temporal development of ε^p is viscoplastically driven by effective stress

$$\mathbf{y} = \mathbf{s} - \mathbf{a}, \tag{1}$$

where $\mathbf{s}$ and $\mathbf{a}$ denote the deviatoric parts of stress σ and back stress α, respectively. We thus consider the following elastic and viscoplastic equations, in which temperature T appears as a state variable:

$$\sigma = \mathbf{D}^e(T) : (\varepsilon^m - \varepsilon^p), \tag{2}$$

$$\dot{\varepsilon}^p = \sqrt{\tfrac{3}{2}}\, g(\overline{y},\ p,\ T)\mathbf{n} \text{ with } \mathbf{n} = \mathbf{y}/\|\mathbf{y}\|, \tag{3}$$

where $\mathbf{D}^e$ indicates elastic stiffness, g is a viscoplastic function, and $\overline{y}$ and p denote the equivalent effective stress and accumulated inelastic strain defined, respectively, as

$$\overline{y} = \sqrt{\tfrac{3}{2}}\,\|\mathbf{y}\|, \tag{4}$$

$$\dot{p} = \sqrt{\tfrac{2}{3}}\,\|\dot{\varepsilon}^p\|. \tag{5}$$

Here, it is noted that neither stress rate nor temperature rate can be, in general, an argument of the viscoplastic function g [Lemaitre and Chaboche (1990)].

For back stress, let us assume the following: (1) back stress consists of several parts, i.e., $\alpha = \sum \alpha^{(i)}$ [Chaboche and Rousselier (1983)], (2) the evolution of each part is caused by strain hardening and *nonlinear* dynamic recovery [Ohno and Wang (1993, 1994); Ohno (1998)], and (3) this evolution has dependence on temperature but no dependence on temperature history [Ohno and Wang (1991); McDowell (1992)]. We thus consider

$$\mathbf{a} = \sum r^{(i)}(T)\mathbf{b}^{(i)}, \tag{6}$$

$$\dot{\mathbf{b}}^{(i)} = \tfrac{2}{3}\xi^{(i)}\dot{\varepsilon}^p - \zeta^{(i)}\mathbf{b}^{(i)}\dot{p}^{(i)}, \tag{7}$$

where $r^{(i)}(T)$ expresses the temperature dependence of back stress evolution, $\mathbf{b}^{(i)}$ is a back stress compensating for temperature dependence, $\xi^{(i)}$ and $\zeta^{(i)}$ are the temperature-independent material parameters for strain hardening and dynamic recovery, respectively, and $\dot{p}^{(i)}$ is an inelastic strain rate causing the dynamic recovery of $\mathbf{b}^{(i)}$. Here and from now on, the superscript (i) will indicate the concern with the ith part of back stress.

As seen from Eqs. 6 and 7, $\mathbf{b}^{(i)}$ is defined up to a numerical factor. This allows us to take $\xi^{(i)} = \zeta^{(i)}$ without loss of generality, so that Eq. 7 becomes

$$\dot{\mathbf{b}}^{(i)} = \zeta^{(i)} \left(\tfrac{2}{3} \dot{\varepsilon}^p - \mathbf{b}^{(i)} \dot{p}^{(i)} \right). \tag{8}$$

The nonlinearity of dynamic recovery is incorporated in $\dot{p}^{(i)}$ so that ratcheting and mean-stress relaxation can be properly simulated. According to Ohno and Wang (1993, 1994), $\dot{p}^{(i)}$ can be written as

$$\dot{p}^{(i)} = (\overline{b}^{(i)})^{k^{(i)}} \dot{p}, \tag{9}$$

where $k^{(i)}$ is a material parameter for the evolution of $\mathbf{b}^{(i)}$, and

$$\overline{b}^{(i)} = \sqrt{\tfrac{3}{2}} \left\| \mathbf{b}^{(i)} \right\|. \tag{10}$$

Then, if $k^{(i)} = 0$, we have $\dot{p}^{(i)} = \dot{p}$, so that Eq. 8 reduces to the Armstrong and Frederick model; if $k^{(i)} = \infty$, Eqs. 8 and 9 render $\dot{p}^{(i)}$ nonzero only in a critical state of $\overline{b}^{(i)} = 1$, leading to the multilinear model derived by Ohno and Wang (1993). Incidentally, these models were discussed using a group-theoretical approach by Liu (2005).

3 Backward Euler discretization

Let us consider the step from a state n to $n+1$. Let us signify the increments in the step by a prefix Δ, and let us denote the constitutive variables at n and $n+1$ by the subscripts n and $n+1$, respectively. Then, using the backward Euler method, the constitutive relations given in the preceding section are discretized as

$$\mathbf{y}_{n+1} = \mathbf{s}_{n+1} - \mathbf{a}_{n+1}, \tag{11}$$

$$\sigma_{n+1} = \mathbf{D}^e(T_{n+1}) : \left(\varepsilon^m_{n+1} - \varepsilon^p_{n+1} \right), \tag{12}$$

$$\varepsilon^p_{n+1} = \varepsilon^p_n + \Delta\varepsilon^p_{n+1}, \tag{13}$$

$$\Delta\varepsilon^p_{n+1} = \sqrt{\tfrac{3}{2}} g(\overline{y}_{n+1},\, p_{n+1},\, T_{n+1}) \mathbf{n}_{n+1} \Delta t_{n+1}, \tag{14}$$

$$\overline{y}_{n+1} = \sqrt{\tfrac{3}{2}} \left\| \mathbf{y}_{n+1} \right\|, \tag{15}$$

$$\mathbf{n}_{n+1} = \sqrt{\tfrac{3}{2}} \mathbf{y}_{n+1} / \overline{y}_{n+1}, \tag{16}$$

$$p_{n+1} = p_n + \Delta p_{n+1}, \tag{17}$$

$$\Delta p_{n+1} = \sqrt{\tfrac{2}{3}} \left\| \Delta\varepsilon^p_{n+1} \right\|, \tag{18}$$

$$\mathbf{a}_{n+1} = \sum r^{(i)}(T_{n+1}) \mathbf{b}^{(i)}_{n+1}, \tag{19}$$

$$\mathbf{b}^{(i)}_{n+1} = \theta^{(i)}_{n+1} \left(\mathbf{b}^{(i)}_n + \tfrac{2}{3} \zeta^{(i)} \Delta\varepsilon^p_{n+1} \right), \tag{20}$$

$$\theta^{(i)}_{n+1} = \left[1 + \zeta^{(i)} (\overline{b}^{(i)}_{n+1})^{k^{(i)}} \Delta p_{n+1} \right]^{-1}, \tag{21}$$

$$\overline{b}^{(i)}_{n+1} = \sqrt{\tfrac{3}{2}} \left\| \mathbf{b}^{(i)}_{n+1} \right\|, \tag{22}$$

where $\Delta t_{n+1} = t_{n+1} - t_n$.

4 Implicit integration

In this section, an implicit integration scheme is developed for the elastic-viscoplastic model described in Section 2. The problem considered here is stated as follows: Given $\Delta\varepsilon^m_{n+1}$, Δt_{n+1} and ΔT_{n+1} in addition to all constitutive variables at n, find σ_{n+1} satisfying the discretized constitutive relations, Eqs. 11-22. The so-called linearization approach is employed to iteratively determine σ_{n+1}.

4.1 Linearization and local iterations

Substitution of Eq. 13 into Eq. 12 gives

$$\sigma_{n+1} = \sigma^*_{n+1} - \mathbf{D}^e_{n+1} : \Delta\varepsilon^p_{n+1}, \tag{23}$$

where $\mathbf{D}^e_{n+1} = \mathbf{D}^e(T_{n+1})$, and σ^*_{n+1} denotes elastic tentative stress

$$\sigma^*_{n+1} = \mathbf{D}^e_{n+1} : (\varepsilon^m_{n+1} - \varepsilon^p_n). \tag{24}$$

The deviatoric part of Eq. 23 is

$$\mathbf{s}_{n+1} = \mathbf{s}^*_{n+1} - \mathbf{I}^d : \mathbf{D}^e_{n+1} : \Delta\varepsilon^p_{n+1}, \tag{25}$$

where $\mathbf{s}^*_{n+1}$ is the deviatoric part of σ^*_{n+1}, and $\mathbf{I}^d$ indicates the following deviatoric operator defined in terms of the fourth and second rank unit tensors, $\mathbf{I}$ and 1:

$$\mathbf{I}^d = \mathbf{I} - \tfrac{1}{3}(1 \otimes 1). \tag{26}$$

Then, subtracting $\mathbf{a}_{n+1}$ from the both sides in Eq. 25, and using Eqs. 11 and 19, we have

$$\mathbf{y}_{n+1} = \mathbf{s}^*_{n+1} - \mathbf{I}^d : \mathbf{D}^e_{n+1} : \Delta\varepsilon^p_{n+1} - \sum r^{(i)}_{n+1} \mathbf{b}^{(i)}_{n+1}, \tag{27}$$

where $r^{(i)}_{n+1} = r^{(i)}(T_{n+1})$.

The above equation can be regarded as a nonlinear tensor equation to determine $\mathbf{y}_{n+1}$, because $\Delta\varepsilon^p_{n+1}$ and $\mathbf{b}^{(i)}_{n+1}$ nonlinearly depend on $\mathbf{y}_{n+1}$ and $\Delta\varepsilon^p_{n+1}$, respectively, as seen from Eqs. 14-18 and 20-22. Here it is noted that ε^m_{n+1}, T_{n+1} and Δt_{n+1} are known, since they are prescribed in the integration from n to $n+1$, as aforementioned. Thus, let us linearize Eq. 27 as

$$\begin{aligned}&\mathbf{y}_{n+1}+d\mathbf{y}_{n+1}\\&\quad=\mathbf{s}^*_{n+1}-\mathbf{I}^d:\mathbf{D}^e_{n+1}:(\Delta\varepsilon^p_{n+1}+d\Delta\varepsilon^p_{n+1})\\&\quad-\sum r^{(i)}_{n+1}(\mathbf{b}^{(i)}_{n+1}+d\mathbf{b}^{(i)}_{n+1}),\end{aligned}\tag{28}$$

and let us suppose that $d\Delta\varepsilon^p_{n+1}$ and $d\mathbf{b}^{(i)}_{n+1}$ are represented as

$$d\Delta\varepsilon^p_{n+1}=\mathbf{P}_{n+1}:d\mathbf{y}_{n+1},\tag{29}$$

$$d\mathbf{b}^{(i)}_{n+1}=\mathbf{H}^{(i)}_{n+1}:d\Delta\varepsilon^p_{n+1},\tag{30}$$

where $\mathbf{P}_{n+1}$ and $\mathbf{H}^{(i)}_{n+1}$ are fourth rank tensors (see Section 6). Substitution of Eqs. 29 and 30 into Eq. 28 gives

$$\mathbf{A}_{n+1}:d\mathbf{y}_{n+1}=\lambda_{n+1},\tag{31}$$

where

$$\mathbf{A}_{n+1}=\mathbf{I}+\left(\mathbf{I}^d:\mathbf{D}^e_{n+1}+\sum r^{(i)}_{n+1}\mathbf{H}^{(i)}_{n+1}\right):\mathbf{P}_{n+1},\tag{32}$$

$$\lambda_{n+1}=\mathbf{s}^*_{n+1}-\mathbf{y}_{n+1}-\mathbf{I}^d:\mathbf{D}^e_{n+1}:\Delta\varepsilon^p_{n+1}-\sum r^{(i)}_{n+1}\mathbf{b}^{(i)}_{n+1}.\tag{33}$$

By solving Eq. 31 for $d\mathbf{y}_{n+1}$, $\mathbf{y}_{n+1}$ is updated to $\mathbf{y}_{n+1}+d\mathbf{y}_{n+1}$ so that $\mathbf{y}_{n+1}$ can be iteratively determined. This iteration method is expected to have quadratic convergence, because it is based on the linearization as in the Newton-Raphson method. Thus, σ_{n+1} can be computed after iteratively determining $\mathbf{y}_{n+1}$ as well as $\Delta\varepsilon^p_{n+1}$ and $\mathbf{b}^{(i)}_{n+1}$ as follows:

(1) Estimate the initial value of $\mathbf{y}_{n+1}$ (Section 4.2).

(2) Evaluate $\Delta\varepsilon^p_{n+1}$ by inputting $\mathbf{y}_{n+1}$ to Eqs. 14-18.

(3) Evaluate $\mathbf{b}^{(i)}_{n+1}$ by inputting $\Delta\varepsilon^p_{n+1}$ to Eqs. 20-22.

(4) Compute $\mathbf{P}_{n+1}$ and $\mathbf{H}^{(i)}_{n+1}$ using Eqs. 52 and 59.

(5) Solve Eq. 31 for $d\mathbf{y}_{n+1}$.

(6) If $d\mathbf{y}_{n+1}$ satisfies the convergence condition for $\mathbf{y}_{n+1}$, go to step (8). [3]

(7) Update $\mathbf{y}_{n+1}$ to $\mathbf{y}_{n+1}+d\mathbf{y}_{n+1}$, and go to step (2).

(8) Compute σ_{n+1} using Eqs. 23 and 24.

In step (2), Δp_{n+1} needs to be evaluated using the following equation, if p_{n+1} appears in the function g in Eq. 14:

$$\Delta p_{n+1}=g(\overline{y}_{n+1},\ p_n+\Delta p_{n+1},\ T_{n+1})\Delta t_{n+1}.\tag{34}$$

Moreover, if $k^{(i)}\neq 0$, it is necessary to figure $\overline{b}^{(i)}_{n+1}$ in advance in step (3) using the following equation based on Eqs. 20-22:

$$\left[1+\zeta^{(i)}(\overline{b}^{(i)}_{n+1})^{k^{(i)}}\Delta p_{n+1}\right]\overline{b}^{(i)}_{n+1}=\sqrt{\tfrac{3}{2}}\left\|\mathbf{b}^{(i)}_n+\tfrac{2}{3}\zeta^{(i)}\Delta\varepsilon^p_{n+1}\right\|.\tag{35}$$

The iterations based on steps (1)-(8), which are performed at each integration point in finite elements, will be referred to as *local iterations* henceforth, while the iterations to solve nodal force equilibrium equations will be called *global iterations*.

4.2 Initial value in local iterations

The initial value of $\mathbf{y}_{n+1}$, $\mathbf{y}^0_{n+1}$, in local iterations is estimated by assuming $\Delta\varepsilon^m_{n+1}$ to be either elastic or viscoplastic. If $\Delta\varepsilon^m_{n+1}$ is assumed to be elastic, we have

$$\mathbf{y}^{0e}_{n+1}=\mathbf{s}^*_{n+1}-\mathbf{a}_n(T_{n+1}),\tag{36}$$

where $\mathbf{s}^*_{n+1}$ is given by the deviatoric part of Eq. 24, and $\mathbf{a}_n(T_{n+1})=\sum r^{(i)}(T_{n+1})\mathbf{b}^{(i)}_n$. On the other hand, if $\Delta\varepsilon^m_{n+1}$ is completely viscoplastic, we have

$$\mathbf{y}^{0v}_{n+1}=\sqrt{\tfrac{2}{3}}\overline{y}^{0v}_{n+1}\mathbf{I}^d:\Delta\varepsilon^m_{n+1}\Big/\left\|\mathbf{I}^d:\Delta\varepsilon^m_{n+1}\right\|.\tag{37}$$

Here $\overline{y}^{0v}_{n+1}$ is obtained from the following equation based on Eq. 14 with $\Delta\varepsilon^p_{n+1}$ replaced by $\mathbf{I}^d:\Delta\varepsilon^m_{n+1}$:

$$\begin{aligned}\sqrt{\tfrac{2}{3}}\left\|\mathbf{I}^d:\Delta\varepsilon^m_{n+1}\right\|&=g(\overline{y}^{0v}_{n+1},\ p_n\\&+\sqrt{\tfrac{2}{3}}\left\|\mathbf{I}^d:\Delta\varepsilon^m_{n+1}\right\|,\ T_{n+1})\Delta t_{n+1}.\end{aligned}\tag{38}$$

The Euclidean norms of $\mathbf{y}^{0e}_{n+1}$ and $\mathbf{y}^{0v}_{n+1}$ are then compared to choose the smaller one as $\mathbf{y}^0_{n+1}$ between the two.

[3] In the case of no convergence after a prescribed number of iterations, a warning message is generated, and step (8) is coerced.

5 Consistent tangent modulus

Fourth rank tensors $\mathbf{P}_{n+1}$ and $\mathbf{H}^{(i)}_{n+1}$ have been introduced to represent $d\Delta\varepsilon^p_{n+1}$ and $d\mathbf{b}^{(i)}_{n+1}$, respectively, in the last section. Here, by following a previous study [Kobayashi et al. (2003)], it is shown that these tensors are readily incorporated in deriving consistent tangent modulus $\partial\sigma_{n+1}\big/\partial\Delta\varepsilon^m_{n+1}$.

Let us consider the variations in discretized variables due to the change in $\Delta\varepsilon^m_{n+1}$, $d\Delta\varepsilon^m_{n+1}$. Here it is noted that no variations in T_{n+1} and Δt_{n+1} need to be considered for deriving $\partial\sigma_{n+1}\big/\partial\Delta\varepsilon^m_{n+1}$. Then, Eqs. 23-25 provide

$$d\sigma_{n+1} = \mathbf{D}^e_{n+1} : d\Delta\varepsilon^m_{n+1} - \mathbf{D}^e_{n+1} : d\Delta\varepsilon^p_{n+1}, \tag{39}$$

$$d\mathbf{s}_{n+1} = \mathbf{I}^d : \mathbf{D}^e_{n+1} : (d\Delta\varepsilon^m_{n+1} - d\Delta\varepsilon^p_{n+1}). \tag{40}$$

Moreover, substitution of Eq. 11 into Eq. 29 gives

$$d\Delta\varepsilon^p_{n+1} = \mathbf{P}_{n+1} : (d\mathbf{s}_{n+1} - d\mathbf{a}_{n+1}). \tag{41}$$

Eqs. 19 and 30 allow the above equation to become

$$\mathbf{M}_{n+1} : d\Delta\varepsilon^p_{n+1} = \mathbf{P}_{n+1} : d\mathbf{s}_{n+1}, \tag{42}$$

where

$$\mathbf{M}_{n+1} = \mathbf{I} + \mathbf{P}_{n+1} : \sum r^{(i)}_{n+1}\mathbf{H}^{(i)}_{n+1}. \tag{43}$$

By further substituting Eq. 40 into Eq. 42, and by arranging the resulting equation, we have

$$d\Delta\varepsilon^p_{n+1} = (\mathbf{M}_{n+1} + \mathbf{P}_{n+1} : \mathbf{I}^d : \mathbf{D}^e_{n+1})^{-1} : \mathbf{P}_{n+1} : \mathbf{I}^d : \mathbf{D}^e_{n+1} : d\Delta\varepsilon^m_{n+1}. \tag{44}$$

Eqs. 39 and 44 then give

$$\frac{\partial\sigma_{n+1}}{\partial\Delta\varepsilon^m_{n+1}} = \mathbf{D}^e_{n+1} : \left[\mathbf{I} - (\mathbf{M}_{n+1} + \mathbf{P}_{n+1} : \mathbf{I}^d : \mathbf{D}^e_{n+1})^{-1} : \mathbf{P}_{n+1} : \mathbf{I}^d : \mathbf{D}^e_{n+1}\right]. \tag{45}$$

This consistent tangent modulus reduces to that derived by Kobayashi et al. (2003), if $\mathbf{D}^e_{n+1}$ is isotropic.

6 Derivation of $\mathbf{P}_{n+1}$ and $\mathbf{H}^{(i)}_{n+1}$

This section deals with deriving $\mathbf{P}_{n+1}$ and $\mathbf{H}^{(i)}_{n+1}$, defined in Eqs. 29 and 30, which have been assumed for the implicit integration and consistent tangent modulus in Sections 4 and 5.

Differentiation of Eqs. 14-18 under no variations of T_{n+1} and Δt_{n+1} gives

$$d\Delta\varepsilon^p_{n+1} = \sqrt{\tfrac{3}{2}}\,(dg_{n+1}\mathbf{n}_{n+1} + g_{n+1}d\mathbf{n}_{n+1})\,\Delta t_{n+1}, \tag{46}$$

$$d\mathbf{n}_{n+1} = \sqrt{\tfrac{3}{2}}d\mathbf{y}_{n+1}\big/\overline{y}_{n+1} - (\mathbf{n}_{n+1}\big/\overline{y}_{n+1})d\overline{y}_{n+1}, \tag{47}$$

$$d\overline{y}_{n+1} = \sqrt{\tfrac{3}{2}}\mathbf{n}_{n+1} : d\mathbf{y}_{n+1}. \tag{48}$$

$$d\Delta p_{n+1} = dg_{n+1}\Delta t_{n+1}, \tag{49}$$

where $g_{n+1} = g(\overline{y}_{n+1},\ p_{n+1},\ T_{n+1})$, and

$$dg_{n+1} = (\partial g_{n+1}/\partial\overline{y}_{n+1})d\overline{y}_{n+1} + (\partial g_{n+1}/\partial p_{n+1})d\Delta p_{n+1}. \tag{50}$$

Thus, we have

$$d\Delta\varepsilon^p_{n+1} = \mathbf{P}_{n+1} : d\mathbf{y}_{n+1}, \tag{51}$$

where

$$\mathbf{P}_{n+1} = \frac{3}{2}\left[\frac{g_{n+1}}{\overline{y}_{n+1}}(\mathbf{I} - \mathbf{n}_{n+1}\otimes\mathbf{n}_{n+1}) + \left(1 - \frac{\partial g_{n+1}}{\partial p_{n+1}}\Delta t_{n+1}\right)^{-1}\frac{\partial g_{n+1}}{\partial\overline{y}_{n+1}}\,\mathbf{n}_{n+1}\otimes\mathbf{n}_{n+1}\right]\Delta t_{n+1}. \tag{52}$$

Moreover, differentiation of Eqs. 20 and 21 provides

$$d\mathbf{b}^{(i)}_{n+1} = \left(d\theta^{(i)}_{n+1}/\theta^{(i)}_{n+1}\right)\mathbf{b}^{(i)}_{n+1} + \tfrac{2}{3}\zeta^{(i)}\theta^{(i)}_{n+1}d\Delta\varepsilon^p_{n+1}, \tag{53}$$

$$d\theta^{(i)}_{n+1}\Big/\theta^{(i)}_{n+1} = -\zeta^{(i)}\theta^{(i)}_{n+1}\left(\omega^{(i)}_{n+1}d\Delta p_{n+1} + \Delta p_{n+1}\hat{\omega}^{(i)}_{n+1}d\overline{b}^{(i)}_{n+1}\right), \tag{54}$$

where $\omega^{(i)}_{n+1} = (\overline{b}^{(i)}_{n+1})^{k^{(i)}}$ and $\hat{\omega}^{(i)}_{n+1} = d\omega^{(i)}_{n+1}\Big/d\overline{b}^{(i)}_{n+1}$. Here, using Eqs. 18 and 22, it is shown that

$$d\Delta p_{n+1} = \sqrt{\tfrac{2}{3}}\mathbf{n}_{n+1} : d\Delta\varepsilon^p_{n+1}, \tag{55}$$

$$d\overline{b}^{(i)}_{n+1} = \tfrac{3}{2}\mathbf{b}^{(i)}_{n+1} : d\mathbf{b}^{(i)}_{n+1}\Big/\overline{b}^{(i)}_{n+1}. \tag{56}$$

Then, substituting Eqs. 55 and 56 into Eq. 54, and using Eq. 53, we have

$$\frac{d\theta_{n+1}^{(i)}}{\theta_{n+1}^{(i)}} = -\frac{\zeta^{(i)}\theta_{n+1}^{(i)}}{\left(1+\zeta^{(i)}\theta_{n+1}^{(i)}\hat{\omega}_{n+1}^{(i)}\Delta p_{n+1}\overline{b}_{n+1}^{(i)}\right)\overline{b}_{n+1}^{(i)}} \times \left(\sqrt{\tfrac{2}{3}}\omega_{n+1}^{(i)}\overline{b}_{n+1}^{(i)}\mathbf{n}_{n+1} : d\Delta\varepsilon_{n+1}^{p} + \zeta^{(i)}\theta_{n+1}^{(i)}\hat{\omega}_{n+1}^{(i)}\Delta p_{n+1}\mathbf{b}_{n+1}^{(i)} : d\Delta\varepsilon_{n+1}^{p}\right). \quad (57)$$

Consequently, Eqs. 53 and 57 give

$$d\mathbf{b}_{n+1}^{(i)} = \mathbf{H}_{n+1}^{(i)} : d\Delta\varepsilon_{n+1}^{p}, \quad (58)$$

Table 1 : Material parameters (stress in MPa, strain in mm/mm, time in s, and temperature in ˚C)

Young's modulus
$E = 1.07\times10^{5} + 2.72\times10^{2}(T+273.15)$
$-0.24(T+273.15)^{2}$
Poisson's ratio
$\nu = 0.3$
Coefficient of thermal expansion
1.52×10^{-5}
Viscoplastic function
$g = 1.0\times10^{-3}\left[3.19\times10^{-3}\overline{\sigma}/\phi(T)\right]^{m(T)}$
$m(T) = 120\left\{8.0\times10^{6}\exp\left[-1.23\times 10^{4}/(T+273.15)\right]+1\right\}^{-1}$
$\phi(T) = \left\{3.27\times10^{5}\exp\left[-1.21\times 10^{4}/(T+273.15)\right]+1\right\}^{-1}$
Kinematic hardening parameters
$\zeta^{(1)} = 4000 \quad r^{(1)} = 25.0\phi(T)$
$\zeta^{(2)} = 1000 \quad r^{(2)} = 24.4\phi(T)$
$\zeta^{(3)} = 500 \quad r^{(3)} = 21.2\phi(T)$
$\zeta^{(4)} = 200 \quad r^{(4)} = 20.5\phi(T)$
$\zeta^{(5)} = 100 \quad r^{(5)} = 31.7\phi(T)$
$k^{(i)} = 5 \quad (i = 1,2,\cdots,5)$

where

$$\mathbf{H}_{n+1}^{(i)} = \zeta^{(i)}\theta_{n+1}^{(i)} \times \left[\frac{2}{3}\mathbf{I} - \frac{\sqrt{\tfrac{2}{3}}\omega_{n+1}^{(i)}\overline{b}_{n+1}^{(i)}\mathbf{b}_{n+1}^{(i)}\otimes\mathbf{n}_{n+1} + \zeta^{(i)}\theta_{n+1}^{(i)}\hat{\omega}_{n+1}^{(i)}\Delta p_{n+1}\mathbf{b}_{n+1}^{(i)}\otimes\mathbf{b}_{n+1}^{(i)}}{\left(1+\zeta^{(i)}\theta_{n+1}^{(i)}\hat{\omega}_{n+1}^{(i)}\Delta p_{n+1}\overline{b}_{n+1}^{(i)}\right)\overline{b}_{n+1}^{(i)}}\right]. \quad (59)$$

7 Numerical examples

The implicit integration scheme, as well as consistent tangent modulus, developed in the present study was programmed as a user subroutine UMAT in version 6.5 of the ABAQUS code. In the programming, the initial value of $\mathbf{y}_{n+1}$ in local iterations was chosen by assuming $\Delta\varepsilon_{n+1}^{m}$ to be either elastic or viscoplastic (Section 4.2), and the convergence condition of local iterations was set as

$$\|d\mathbf{y}_{n+1}\| / \|\mathbf{y}_{n+1}\| < 10^{-6}. \quad (60)$$

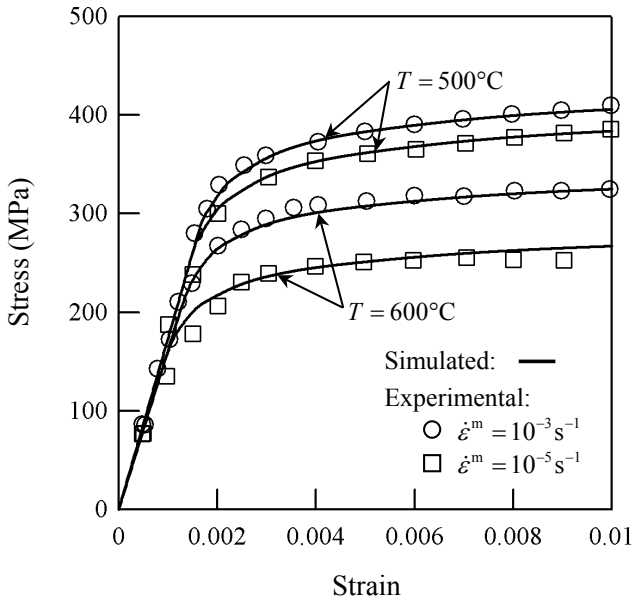

Figure 1 : Tensile stress-strain curves of $2^{1}/_{4}$Cr-1Mo steel at 500 and 600 ˚C; experiments by Iwasaki, Hiroe and Igari (1987).

Finite element analysis has been thus performed to show numerical examples. The material parameters employed for the numerical examples are listed in Tab. 1. They were determined by applying the multilinear approximation of tensile stress-strain curves [Jiang and Sehitoglu (1996); Ohno (1998, 2001)] to the tensile test data of $2^{1}/_{4}$Cr-1Mo steel at 300-600 ˚C [Iwasaki, Hiroe and Igari (1987); Ohno and Wang (1992)]. Here it is noted that this material exhibits negligible cyclic hardening/softening as far as the first several cycles are concerned, and that a typical value of $k^{(i)}$ is around five [Ohno and Wang (1993, 1994); Jiang and Sehitoglu (1996)]. The tensile experiments were then successfully simulated (Figs. 1 and 2).

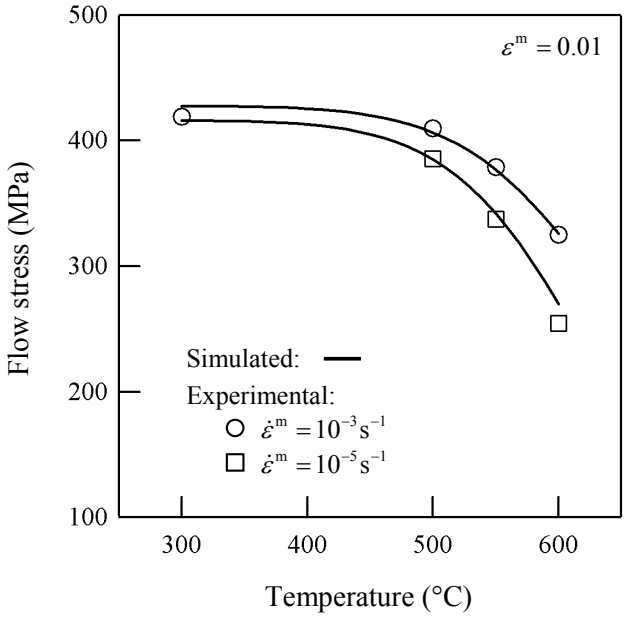

Figure 2 : Viscoplastic flow stresses of $2^1/_4$Cr-1Mo steel at $\varepsilon^m = 0.01$; experiments by Iwasaki, Hiroe and Igari (1987).

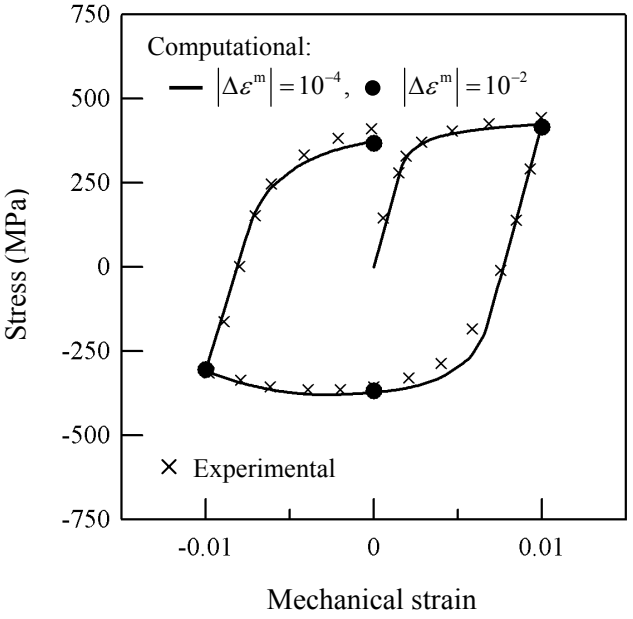

Figure 4 : Stress versus mechanical strain relation under out-of-phase change in ε^m and T; experiment by Iwasaki, Hiroe and Igari (1987).

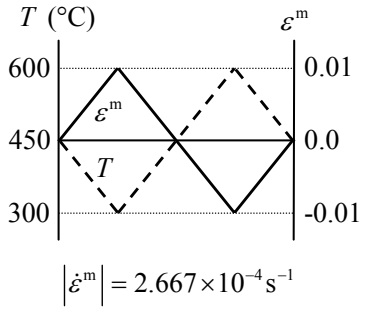

Figure 3 : Out-of-phase change in mechanical strain ε^m and temperature T.

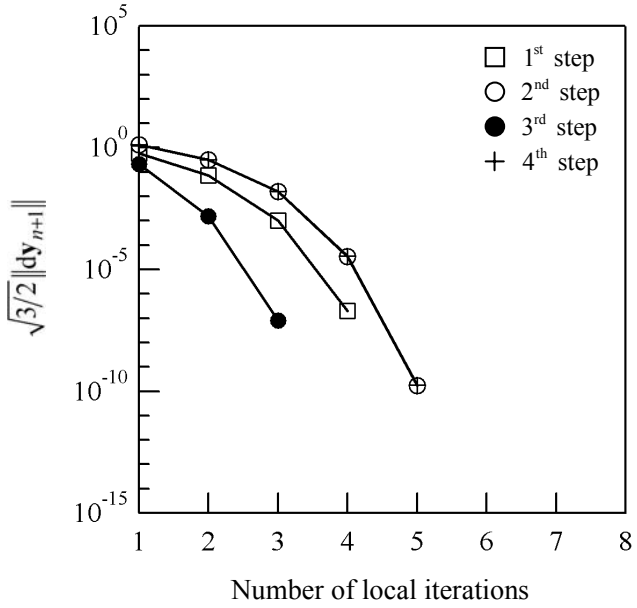

Figure 5 : Variation in $\sqrt{\frac{3}{2}}\,\|\mathbf{dy}_{n+1}\|$ with the number of local iterations in the case of $|\Delta\varepsilon^m| = 10^{-2}$ under out-of-phase change in ε^m and T.

First, the implicit integration scheme described in Section 4 was verified by analyzing a simple uniaxial problem, in which a straight bar with a uniform cross-section was subjected to the out-of-phase variation in ε^m and T depicted in Fig. 3. The bar was modeled using one 8-node liner brick element, C3D8, and the change in nodal displacement was prescribed so as to produce the variation in ε^m given in Fig. 3. The computation then pro-

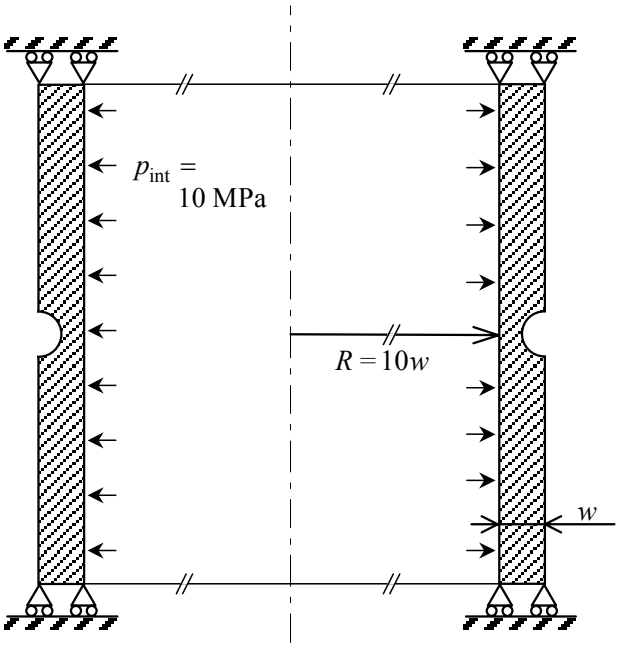

(a)

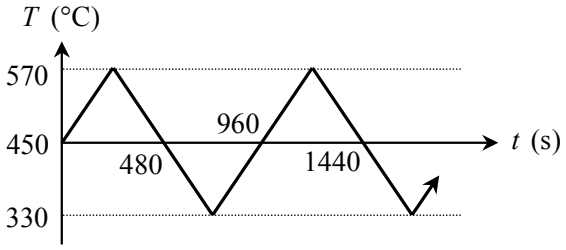

(b)

Figure 6 : (a) axisymmetric circular-notched tube with axial displacement constraint at ends, and (b) temperature cycling applied to circular-notched tube.

vided the nonisothermal σ versus ε^m relation close to the experiment done by Iwasaki, Hiroe and Igari (1987), as shown in Fig. 4. The computation was performed in two cases of $|\Delta\varepsilon^m| = 10^{-4}$ and 10^{-2}. It is emphasized that the increment in the latter case was considerably large. Nevertheless, almost the same stresses were obtained in the two cases (Fig. 4). Fig. 5 illustrates how the local iterations for implicit integration converged in the case of $|\Delta\varepsilon^m| = 10^{-2}$. The convergence condition of local iterations was always satisfied even in this case. It is seen from the Fig. 5 that the local iterations had quadratic convergence. Such quick convergence was expected, because the local iterations are based on the linearlization as in the Newton-Raphson method (Section 4.1). We therefore can say that the implicit integration scheme developed in this study allows us to take large increments, and that the iteration method introduced in the implicit integration scheme affords quadratic convergence.

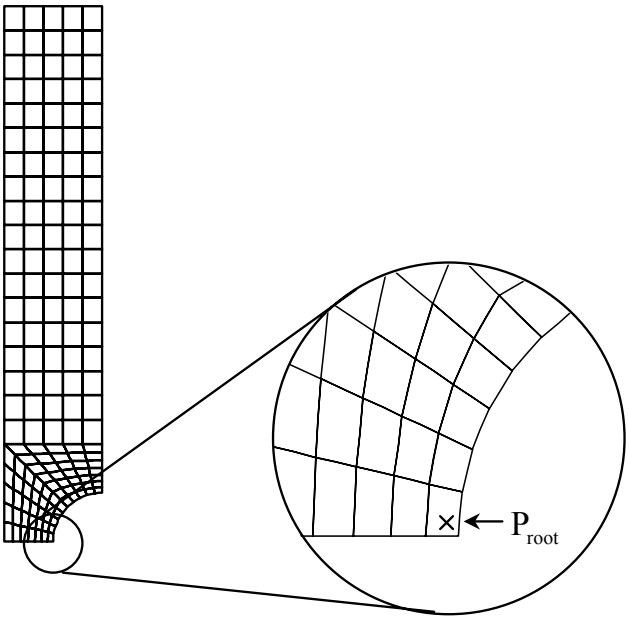

Figure 7 : Finite element mesh of a quarter of vertical cross-section of circular notched tube.

The implicit integration scheme was then examined further by analyzing a nonuniform structure subjected to thermal-mechanical cyclic loading. Ratcheting in such a structure was of interest because of the nonlinearity of dynamic recovery in Eq. 8. We thus analyzed an axisymmetric circular-notched tube, with axial displacement constraint at both ends, subjected to an internal pressure p_{int} and uniform variations in T; while p_{int} was kept constant at 10 MPa, T was cyclically varied twenty times between 330 and 570 °C (Fig. 6). A quarter of the vertical cross-section of the tube was divided into finite elements using 8-node biquadratic reduced integration elements, CAX8R, as shown in Fig. 7. The analysis was done by assuming $k^{(i)} = 0$ as well as $k^{(i)} = 5$ to discuss the influence of $k^{(i)}$ on ratcheting. Let us remember that $k^{(i)}$ represents the nonlinearity of dynamic recovery

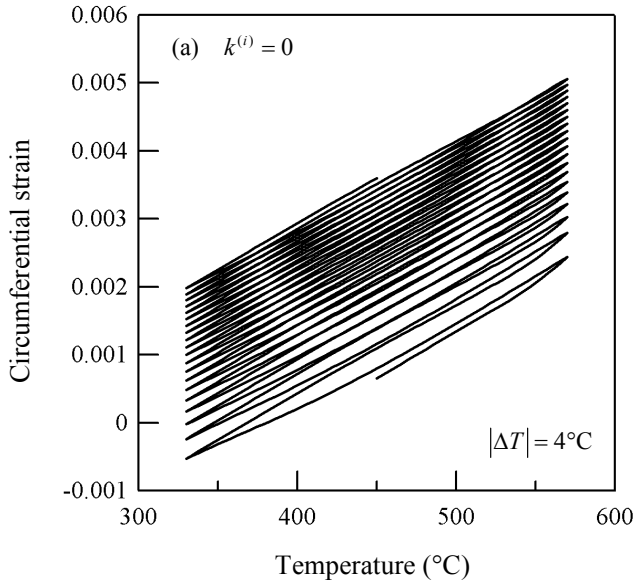

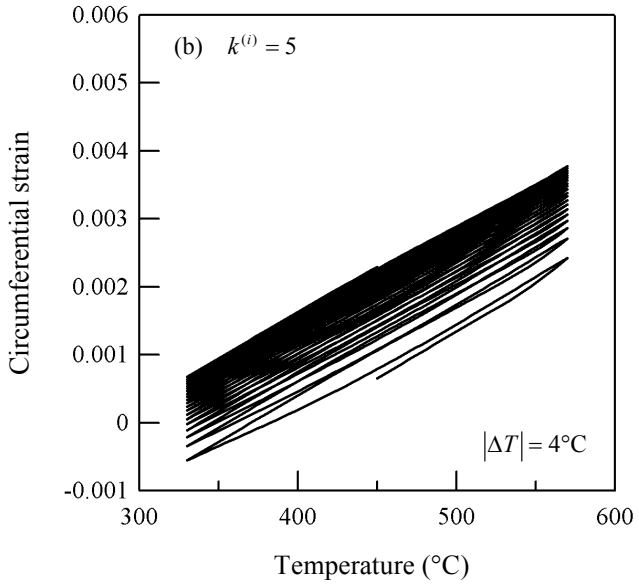

Figure 8 : Change in circumferential strain ε_θ at P_{root} under combined constant internal pressure and temperature cycling; (a) $k^{(i)} = 0$, (b) $k^{(i)} = 5$.

in the evolution of back stresses (Section 2).

When $k^{(i)} = 0$ and 5, circumferential strain ε_θ had the changes shown in Figs. 8(a) and 8(b), respectively, at the integration point closest to the notch root, P_{root}. The computations were performed by taking an increment of $|\Delta T|$ =4 ˚C. It is seen from the figures that ε_θ progressively increased with the number of temperature cycles,

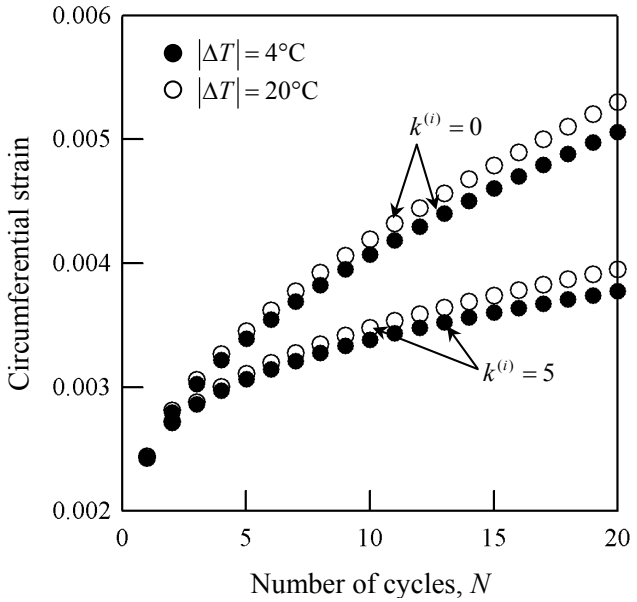

Figure 9 : Increase in circumferential strain ε_θ at temperature peak of 570 ˚C.

N, and that this ratcheting significantly depended on $k^{(i)}$. It is emphasized that the two values of $k^{(i)}$ resulted in a large difference with respect to ratcheting rate, i.e., the increase in ε_θ per cycle; at $N = 20$, the ratcheting rate by $k^{(i)} = 0$ was about 2.5 times larger than that by $k^{(i)}$ =5 (Fig. 9). Further computations were done by taking a larger increment of $|\Delta T|$ =20 ˚C instead of $|\Delta T|$ =4 ˚C. The ratcheting was then hardly influenced in either case of $k^{(i)} = 0$ or 5 (Fig. 9), though the number of steps per cycle was reduced from 120 to 24 in the finite element analysis. The implicit integration scheme was thus successful in efficiently computing ratcheting in the circular-notched tube.

Finally, let us discuss the local and global iterations performed in the analysis of the circular-notched tube. The local iterations, which always converged in the analysis, were monitored at P_{root} in the first temperature cycle. The local iterations then converged after 3.3 and 3.9 iterations, on average, when $|\Delta T|$ =4 and 20 ˚C, respectively, as shown in Fig. 10. It was thus suggested that the magnitude of $|\Delta T|$ did not have a noticeable influence on the convergence of local iterations. The convergence of global iterations was also checked in the first cycle by assuming the default convergence condition of ABAQUS. It was then found that the magnitude of $|\Delta T|$ had a considerable influence on the convergence of global itera-

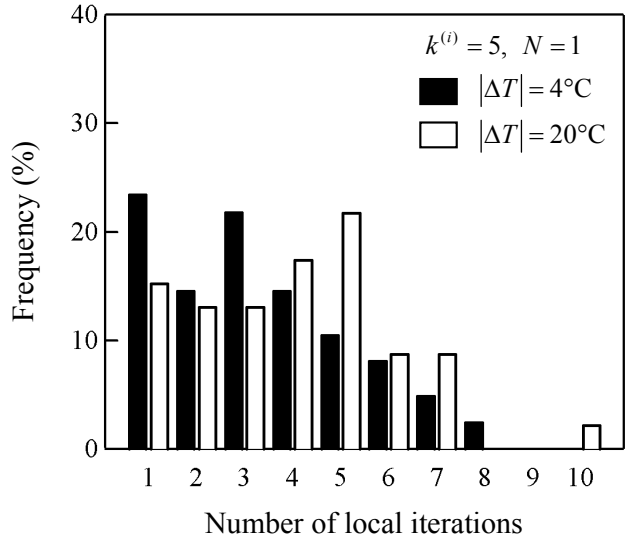

Figure 10 : Number of local iterations for convergence monitored at P_{root} in the first temperature cycle.

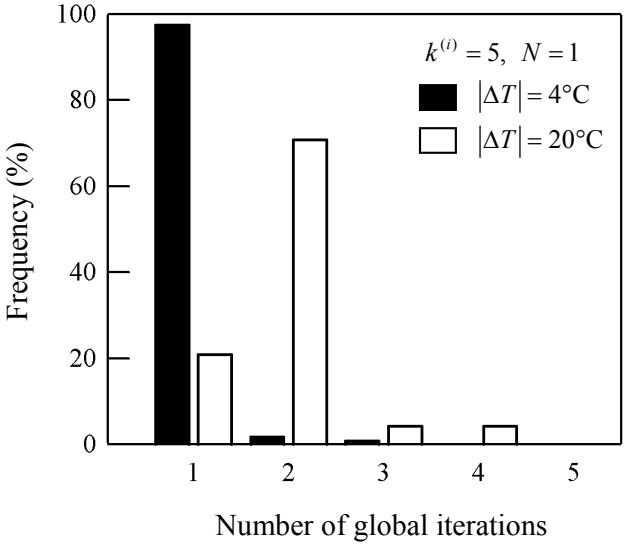

Figure 11 : Number of global iterations for convergence in the first temperature cycle.

tions: the average number of global iterations was 1.0 and 1.9, when $|\Delta T|$ =4 and 20 ˚ C, respectively, as illustrated in Fig. 11. It is, however, noted that whereas the number of global iterations was almost doubled, the increment in finite element analysis, $|\Delta T|$, was quintupled, resulting in a nearly 60 percent reduction in CPU time. Fig. 12 shows how the maximum residual nodal force decreased with the number of global iterations in the case

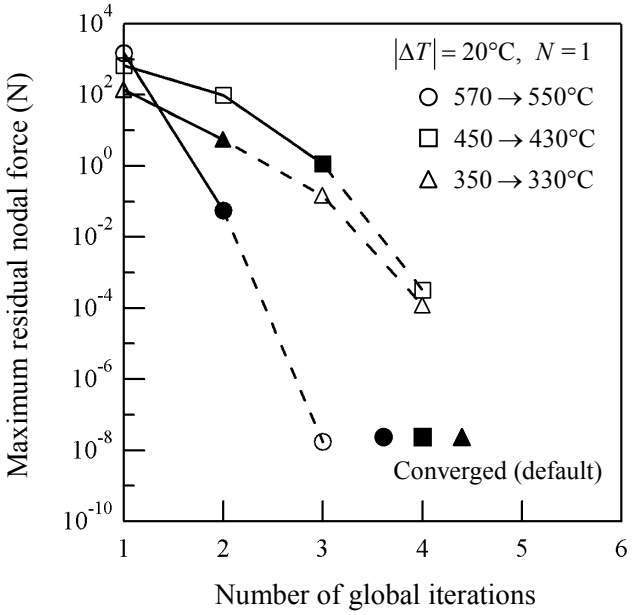

Figure 12 : Examples of change in maximum residual nodal force with the number of global iterations in the case of $|\Delta T|$ =20 ˚ C.

of $|\Delta T|$ =20 ˚ C. As seen from the figure, the global iterations had quadratic convergence, demonstrating the validity of the consistent tangent modulus derived in Section 5. The local and global iterations were thus found to converge well in the analysis of the circular-notched tube.

8 Conclusions

In this study, a fully implicit integration scheme was developed for a nonisothermal viscoplastic, nonlinear kinematic hardening model with multiple back stresses. Nonlinear dynamic recovery in addition to strain hardening was assumed for the evolution of each back stress to simulate well ratcheting and mean-stress relaxation. Temperature dependence of back stress evolution was also taken into account in the constitutive model. The backward Euler discretization of such sophisticated constitutive relations resulted in a tensor equation. Then, to iteratively achieve the implicit integration of constitutive variables, the tensor equation was linearized by introducing the derivatives of discretized inelastic strain and back stresses. These derivatives were shown to be readily incorporated in consistent tangent modulus. The implicit integration scheme and consistent tangent mod-

ulus developed were programmed as a user subroutine UMAT in the ABAQUS code. Then, a straight bar and a circular-notched tube subjected to nonisothermal cyclic loading were analyzed as numerical examples. It was thus demonstrated that the implicit integration scheme allows us to take large increments, and that the iterations in the scheme converge quadratically.

References

Armstrong, P. J.; Frederick, C. O. (1966): A mathematical representation of the multiaxial Bauschinger effect. *CEGB Report RD/B/N731*, Berkeley Nuclear Laboratories, Berkeley, UK.

Chaboche, J. L. (1986): Time-independent constitutive theories for cyclic plasticity. *Int J Plasticity*, vol. 2, pp. 149-188.

Chaboche, J. L. (1991): On some modifications of kinematic hardening to improve the description of ratchetting effects. *Int J Plasticity*, vol. 7, pp. 661-678.

Chaboche, J. L.; Rousselier, G. (1983): On the plastic and viscoplastic constitutive equations, Part I: rules developed with internal variable concept. *ASME J Pressure Vessel Technol*, vol. 105, pp. 153-158.

Doghri, I. (1993): Fully implicit integration and consistent tangent modulus in elasto-plasticity. *Int J Numer Meth Engng*, vol. 36, pp. 3915-3932.

Hartmann, S.; Lührs, G.; Haupt P. (1997): An efficient stress algorithm with applications in viscoplasticity and plasticity. *Int J Numer Meth Engng*, vol. 40, pp. 991-1013.

Hartmann, S.; Haupt, P. (1993): Stress computation and consistent tangent operator using non-linear kinematic hardening models. *Int J Numer Meth Engng*, vol. 36, pp. 3801-3814.

Hu, W.; Wang, C. H. (2003): The implementation of a constitutive model with weighted dynamic recovery and its application. *Comput Mech*, vol. 31, pp. 445-452.

Iwasaki, Y.; Hiroe, T.; Igari, T. (1987): An application of the viscoplasticity theory to the inelastic analysis at elevated temperatures. *Trans. JSME, Ser. A*, vol. 53, pp. 1838-1843, (in Japanese).

Jiang, Y.; Sehitoglu, H. (1996): Modeling of cyclic ratchetting plasticity, Part II: comparison of model simulations with experiments. *ASME J Appl Mech*, vol. 63, pp. 726-733.

Kobayashi, M.; Mukai, M.; Takahashi, H.; Ohno, N.; Kawakami, T.; Ishikawa, T. (2003): Implicit integration and consistent tangent modulus of a time-dependent non-unified constitutive model. *Int J Numer Meth Engng,* vol. 58, pp. 1523-1543.

Kobayashi, M.; Ohno, N. (2002): Implementation of cyclic plasticity models based on a general form of kinematic hardening. *Int J Numer Meth Engng*, vol. 53, pp. 2217-2238.

Lemaitre, J.; Chaboche, J.-L. (1990): Mechanics of Solid Materials, Cambridge University Press, pp. 253-345.

Liu, C.-S. (2005): Computational applications of the Poincaré group on the elastoplasticity with kinematic hardening. *CMES: Computer Modeling in Engineering & Sciences*, vol. 8, pp. 231-258.

McDowell, D. L. (1992): A nonlinear kinematic hardening theory for cyclic thermoplasticity and thermoviscoplasticity. *Int J Plasticity*, vol. 8, pp. 695-728.

Miers, L. S.; Telles, J. C. F. (2004): A general tangent operator procedure for implicit elastoplastic BEM analysis. *CMES: Computer Modeling in Engineering & Sciences*, vol. 6, pp. 431-439.

Ohno, N. (1990): Recent topics in constitutive modeling of cyclic plasticity and viscoplasticity. *Appl Mech Rev*, vol. 43, pp. 283-295.

Ohno, N. (1998): Constitutive modeling of cyclic plasticity with emphasis on ratchetting. *Int J Mech Sci*, vol. 40, pp. 251-261.

Ohno, N. (2001): Kinematic hardening rule with critical state of dynamic recovery. In: J. Lemaitre (ed) *Handbook of Materials Behavior Models*, Academic Press, San Diego, pp. 232-239.

Ohno, N.; Wang, J.-D. (1991): Transformation of a nonlinear kinematic hardening rule to a multisurface form under isothermal and nonisothermal conditions. *Int J Plasticity*, vol. 7, pp. 879-891.

Ohno, N.; Wang, J.-D. (1992): Nonisothermal constitutive modeling of inelasticity based on bounding surface. *Nucl Eng Des*, vol. 133, pp. 369-381.

Ohno, N.; Wang, J.-D. (1993): Kinematic hardening rules with critical state of dynamic recovery, Part I: formulation and basic features for ratchetting behavior, Part II: application to experiments of ratchetting behavior. *Int J Plasticity*, vol. 9, pp. 375-403.

Ohno, N.; Wang, J.-D. (1994): Kinematic hardening rules for simulation of ratchetting behavior. *Eur J Mech, A/Solids*, vol. 13, pp. 519-531.

Sawyer, J. P. G.; Wang, C. H.; Jones, R. (2001): An implicit algorithm using explicit correctors for the kinematic hardening model with multiple back stresses. *Int J Numer Meth Engng*, vol. 50, pp. 2093-2107.

Simo, J. C.; Hughes, T. J. R. (1998): Computational Inelasticity, Springer, New York.

Simo, J. C.; Taylor, R. L. (1985): Consistent tangent operators for rate-independent elastoplasticity. *Comput Meth Appl Mech Engng*, vol. 48, pp. 101-118.

Simo, J. C.; Taylor, R. L. (1986): A return mapping algorithm for plane stress elastoplasticity. *Int J Numer Meth Engng*, vol. 22, pp. 649-670.

Watanabe, O.; Atluri, S. N. (1986): Internal time, general internal variable, and multi-yield-surface theories of plasticity and creep: a unification of concepts. *Int J Plasticity*, vol. 2, pp. 37-57.